

## Influence of Copper–Sulfur Covalency and Copper–Copper Bonding on Valence Delocalization and Electron Transfer in the Cu<sub>A</sub> Site of Cytochrome *c* Oxidase<sup>||</sup>

Kendra Rose Williams,<sup>†</sup> Daniel R. Gamelin,<sup>†</sup>  
Louis B. LaCroix,<sup>†</sup> Robert P. Houser,<sup>‡</sup> William B. Tolman,<sup>‡</sup>  
Ton C. Mulder,<sup>§</sup> Simon de Vries,<sup>§</sup> Britt Hedman,<sup>\*,†</sup>  
Keith O. Hodgson,<sup>\*,†</sup> and Edward I. Solomon<sup>\*,†</sup>

Department of Chemistry, Stanford University and  
Stanford Synchrotron Radiation Laboratory  
Stanford, California 94305

Department of Chemistry, University of Minnesota  
Minneapolis, Minnesota 55455

Department of Microbiology and Enzymology  
Technical University Delft, 2628 BC Delft, The Netherlands

Received September 13, 1996

Cytochrome *c* oxidase (CcO) participates in cellular respiration by coupling the four-electron reduction O<sub>2</sub> → H<sub>2</sub>O with transmembrane proton pumping.<sup>1</sup> The Cu<sub>A</sub> center of CcO is the first destination in electron transfer (ET) from cytochrome *c* to the Cu<sub>B</sub>-heme a<sub>3</sub> pair, where O<sub>2</sub> reduction occurs. Several similarities exist between Cu<sub>A</sub> and blue-copper sites, including their analogous cupredoxin folds, copper-thiolate ligation, and ET function. In contrast with the monomeric blue-copper sites, however, EPR,<sup>2</sup> EXAFS,<sup>3</sup> and recent X-ray crystal structures<sup>4</sup> have shown that Cu<sub>A</sub> is a delocalized mixed-valence Cu dimer bridged by two cysteine sulfurs (S(Cys)) and, in this regard, more closely resembles the mixed-valence iron–sulfur ET clusters. In this communication, we explore the contributions of Cu–ligand and Cu–Cu bonding to valence delocalization and ET in the Cu<sub>A</sub> site of CcO. Sulfur K-edge X-ray absorption spectroscopy (XAS) provides the first direct experimental probe of copper–sulfur covalency in the half-occupied highest-energy molecular orbital (HOMO) of Cu<sub>A</sub> and two structurally-defined dithiolate-bridged models, delocalized mixed-valence **1**<sup>5a</sup> and dicupric **2**.<sup>5b</sup> The Cu coordination environment of each system is shown in Chart 1. Electronic absorption (Abs) and magnetic circular dichroism (MCD) spectroscopies are used to measure the total inter-ion electronic coupling in Cu<sub>A</sub> and **1** through identification of the Class III mixed-valence  $\psi \rightarrow \psi^*$  transitions.<sup>6</sup> The results from these techniques combine to define the pathways for delocalization in Cu<sub>A</sub> and **1** and to describe the individual Cu–S and Cu–Cu contributions to this process. The S K-edge data additionally reveal significant anisotropic Cu–ligand covalency, permitting comparison of competing N- and S-based ET pathways to and from the Cu<sub>A</sub> site.

<sup>†</sup> Stanford University and/or Stanford Synchrotron Radiation Laboratory.

<sup>‡</sup> University of Minnesota.

<sup>§</sup> Technical University Delft.

<sup>||</sup> This research contains equal contributions from the theses of D.R.G. and K.R.W.

(1) (a) Babcock, G. T.; Wikström, M. *Nature* **1992**, *356*, 301–307. (b) Ramirez, B. E.; Malmström, B. G.; Winkler, J. R.; Gray, H. B. *Proc. Natl. Acad. Sci. U.S.A.* **1995**, *92*, 11949–11951.

(2) (a) Kroneck, P. M. H.; Antholine, W. E.; Rieder, J.; Zumft, W. G. *FEBS Lett.* **1988**, *242*, 70–74. (b) von Wachenfeldt, C.; de Vries, S.; van der Oost, J. *FEBS Lett.* **1994**, *340*, 109–113.

(3) Blackburn, N. J.; Barr, M. E.; Woodruff, W. H.; van der Oost, J.; de Vries, S. *Biochemistry* **1994**, *33*, 10401–10407.

(4) (a) Iwata, S.; Ostermeier, C.; Ludwig, B.; Michel, H. *Nature* **1995**, *376*, 660–669. (b) Tsukihara, T.; Aoyama, H.; Yamashita, E.; Tomizake, T.; Yamaguchi, H.; Shinzawa-Itoh, K.; Nakashima, R.; Yaono, R.; Yoshikawa, S. *Science* **1995**, *269*, 1069–1074. (c) *Ibid.* **1996**, *272*, 1136–1144.

(5) (a) Houser, R. P.; Young, V. G., Jr.; Tolman, W. B. *J. Am. Chem. Soc.* **1996**, *118*, 2101–2102. (b) Houser, R. P.; Halfen, J. A.; Young, V. G., Jr.; Blackburn, N. J.; Tolman, W. B. *J. Am. Chem. Soc.* **1995**, *117*, 10745–10746.

(6) Gamelin, D. R.; Bominaar, E. L.; Mathonière, C.; Kirk, M. L.; Wieghardt, K.; Girerd, J.-J.; Solomon, E. I. *Inorg. Chem.* **1996**, *35*, 4323–4335.

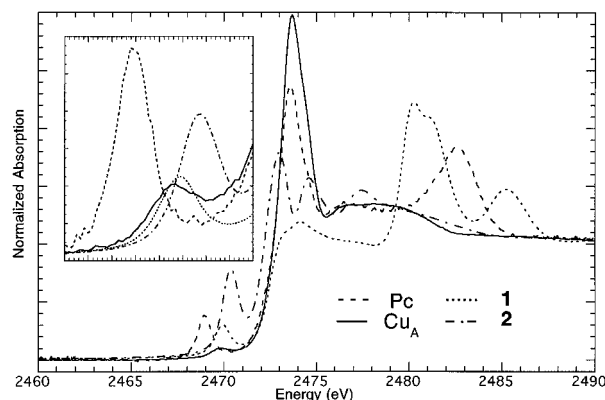
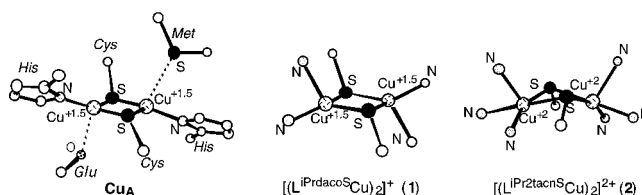


**Figure 1.** S K-edge XAS spectra of Pc,<sup>8</sup> Cu<sub>A</sub>, and models **1** and **2**. Inset: Renormalized pre-edge intensities shown from 2467.5 to 2471.5 eV.

### Chart 1



The normalized S K-edge XAS spectra of **1**, **2**, Cu<sub>A</sub>, and oxidized plastocyanin (Pc) are shown in Figure 1 with the renormalized pre-edge features displayed in the inset.<sup>7</sup> As previously described,<sup>8</sup> the intensity of a S pre-edge absorption feature is directly related to the %S character,  $\alpha^2$ , in the half-occupied HOMO,  $\Psi^* = (1 - \alpha^2)^{1/2}(\text{Cu } 3d) - \alpha(\text{S } 3p)$ . S K-edge and X $\alpha$ -SW results<sup>8</sup> indicate that Pc has a S(Cys) covalency of 38%. Using the Pc covalency as a reference, the %S covalency is found to be 13% in Cu<sub>A</sub>, 14% in **1**, and 25% in **2**. The value obtained for **2** reflects the covalency for each Cu site since both have one d-orbital hole. As there is only one hole shared between the two Cu centers in both Cu<sub>A</sub> and **1**, their covalencies obtained above must be doubled to determine the total HOMO S covalencies, giving congruent values of 26 and 28%, respectively.

Abs and MCD spectra of Cu<sub>A</sub> sites are dominated by three strong features below 25 000 cm<sup>-1</sup>.<sup>2b,11,14</sup> The lowest energy

(7) S K-edge XAS spectra of the *B. subtilis* CcO Cu<sub>A</sub> fragment,<sup>2b</sup> **1**, and **2** were obtained at Stanford Synchrotron Radiation Laboratory (SSRL) as described previously.<sup>8</sup> The monochromator was fully tuned, and the data were collected at 4 °C for Cu<sub>A</sub> and 25 °C for **1** and **2**. The pre-edge intensities have been rescaled by factors of 3 for Pc, 4 for Cu<sub>A</sub>, 1.5 for **1**, and 1 for **2** based on the ratio of total sulfurs present versus the number that contribute to pre-edge intensity. Note that, as with Pc, the long axial S(Met) ligand in Cu<sub>A</sub> has negligible overlap with the equatorial HOMO and therefore does not contribute to pre-edge intensity. The intensities of normalized pre-edge features were quantitated by fits to the data using EDG\_FIT, written by Dr. Graham N. George of SSRL. On the basis of Pc, the error associated with the covalencies is ~3%.<sup>8</sup> 4.2 K Abs and MCD spectra of Cu<sub>A</sub> (50% glycerol-*d*<sub>3</sub> by volume) and **1** (mull) were collected as previously described.<sup>9</sup> X $\alpha$ -SW calculations were performed using the published crystallographic coordinates of **1**<sup>5a</sup> and atomic sphere sizes adapted from experimentally-calibrated Pc calculations.<sup>10</sup>

(8) Shadle, S. E.; Penner-Hahn, J. E.; Schugar, H. J.; Hedman, B.; Hodgson, K. O.; Solomon, E. I. *J. Am. Chem. Soc.* **1993**, *115*, 767–776.

(9) Gamelin, D. R.; Bominaar, E. L.; Kirk, M. L.; Wieghardt, K.; Solomon, E. I. *J. Am. Chem. Soc.* **1996**, *118*, 8085–8097.

(10) Gewirth, A. A.; Solomon, E. I. *J. Am. Chem. Soc.* **1988**, *110*, 3811–3819.

(11) Farrar, J. A.; Lappalainen, P.; Zumft, W. G.; Saraste, M.; Thompson, A. J. *Eur. J. Biochem.* **1995**, *232*, 294–303.

(12) Wallace-Williams, S. E.; James, C. A.; de Vries, S.; Saraste, M.; Lappalainen, P.; van der Oost, J.; Fabian, M.; Palmer, G.; Woodruff, W. H. *J. Am. Chem. Soc.* **1996**, *118*, 3986–3987.

(13) (a) Hush, N. S. *Prog. Inorg. Chem.* **1967**, *8*, 391–444. (b) Marcus, R. A.; Sutin, N. *Biochim. Biophys. Acta* **1985**, *811*, 265–322. (c) Newton, M. D. *Chem. Rev.* **1991**, *91*, 767–792.

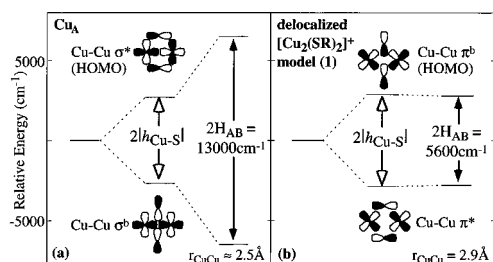


**Figure 2.**  $D_{2h}$ -idealized MO splittings in (a)  $\text{Cu}_A$  and (b) **1**, showing the separate contributions of Cu–S ( $h_{\text{Cu-S}}$ ) and Cu–Cu ( $h_{\text{Cu-Cu}}$ ) bonding interactions to  $2H_{\text{AB}}$ .<sup>21</sup>  $\sigma$  and  $\pi$  labels refer to the symmetries of Cu–Cu interactions only. The specific energies shown result from  $|h_{\text{Cu-S}}| \propto (\alpha(\text{S}))^2$  and  $|h_{\text{Cu-Cu}}(\pi, 2.9 \text{ \AA})|/|h_{\text{Cu-Cu}}(\sigma, 2.5 \text{ \AA})| = 0.01$ . The nonzero value for  $h_{\text{Cu-Cu}}(\pi, 2.9 \text{ \AA})$  is included in b to illustrate that this interaction opposes the effect of superexchange in this splitting.

of these, occurring at  $13\,000 \text{ cm}^{-1}$  in *Bacillus subtilis* CcO,<sup>7</sup> is assigned as the Class III mixed-valence  $\psi \rightarrow \psi^*$  transition<sup>6,9</sup> on the basis of the large change in  $\text{Cu}\cdots\text{Cu}$  separation observed to accompany this excitation in near-IR resonance Raman experiments.<sup>6,12</sup> This transition involves electron promotion between related symmetric and antisymmetric MOs of the delocalized dimer, which leads to resonance enhancement of totally-symmetric Raman vibrations that reflect these bonding changes.<sup>6</sup> In the Class III delocalization limit, this transition energy relates directly to the ground-state electronic-coupling matrix element,  $H_{\text{AB}}$ , which is responsible for valence delocalization:  $E_{\psi \rightarrow \psi^*} = 2H_{\text{AB}}$ .<sup>13</sup>  $2H_{\text{AB}}$  in  $\text{Cu}_A$  is therefore experimentally determined to be  $13\,000 \text{ cm}^{-1}$ . A similar isolated low-energy feature is observed at  $5600 \text{ cm}^{-1}$  in Abs and MCD spectra of **1**<sup>14</sup> and is assigned as the  $\psi \rightarrow \psi^*$  transition in this dimer. This assignment is supported by X $\alpha$ -SW calculations,<sup>5a,7,14</sup> which indicate  $\sim 23\%$  HOMO S covalency and predict this transition to occur at  $4800 \text{ cm}^{-1}$ , with no other dipole-allowed electronic transitions in this region.

From the Abs, MCD, and S K-edge results, MO splitting diagrams are constructed for  $\text{Cu}_A$  (Figure 2a) and **1** (Figure 2b) that describe the independent contributions,  $|h|$ , of Cu–S and Cu–Cu bonding interactions to inter-ion electronic coupling. X $\alpha$ -SW calculations on **1** predict a HOMO involving an in-plane  $\pi$ -bonding combination of Cu monomeric orbitals ( $\pi^b$  with respect to the metals), the  $\pi$ -antibonding combination ( $\pi^*$ ) being filled and at deeper energy (Figure 2b). Significantly, the greater energy of the  $\pi^b$  combination than its  $\pi^*$  counterpart indicates that this splitting in **1** is dominated by Cu–S interactions (since dominant Cu–Cu interactions would result in  $\pi^* > \pi^b$ ) and demonstrates that valence delocalization in **1** is mediated by the bridging ligation rather than by direct Cu–Cu overlap. On the basis of the large Cu–Cu separation in **1** ( $r_{\text{Cu-Cu}} = 2.9 \text{ \AA}$ ) we assume that only ligand contributions to  $H_{\text{AB}}$  are significant in this dimer, such that  $2|h_{\text{Cu-S}}| \approx 2H_{\text{AB}} = 5600 \text{ cm}^{-1}$  (Figure 2b). The similar Cu–S HOMO covalencies measured for **1** (28% S) and  $\text{Cu}_A$  (26% S) (Figure 1) further suggest that the increase of  $2H_{\text{AB}}$  in  $\text{Cu}_A$  to  $13\,000 \text{ cm}^{-1}$  is not due to a large increase in  $|h_{\text{Cu-S}}|$  but is instead due to a direct Cu–Cu bonding interaction ( $|h_{\text{Cu-Cu}}|$ ) resulting from the significantly-shorter Cu–Cu separation in  $\text{Cu}_A$  ( $r_{\text{Cu-Cu}} \approx 2.5 \text{ \AA}$ ). These observations experimentally exclude a  $\pi^b$ – $\pi^*$  delocalization pathway in  $\text{Cu}_A$  analogous to that in **1** (since increasing  $2|h_{\text{Cu-Cu}}|$  in a  $\pi^b$ – $\pi^*$  pathway (Figure 2b) would decrease the experimental  $2H_{\text{AB}}$ ) and implicate instead a  $\sigma^b$ – $\sigma^*$  pathway, for which  $h_{\text{Cu-S}}$  and  $h_{\text{Cu-Cu}}$  contribute with the same sign to  $H_{\text{AB}}$  (Figure 2a). On the basis of the similar Cu–S covalencies in  $\text{Cu}_A$  and **1**, the value of  $2H_{\text{AB}}$  observed in **1** provides an estimate of the superexchange contribution to  $2H_{\text{AB}}$  in  $\text{Cu}_A$  ( $2|h_{\text{Cu-S}}|$  in Figure 2a), while the remaining  $\sim 7400 \text{ cm}^{-1}$  is then attributable to

direct Cu–Cu  $\sigma^b$ – $\sigma^*$  splitting of these orbitals.<sup>15</sup> Therefore, in contrast with delocalization in **1**, which is mediated exclusively by the sulfur bridges (Figure 2b), the pathway for delocalization in  $\text{Cu}_A$  is seen to contain comparable contributions from both Cu–Cu and Cu–S interactions. These results provide a basis for understanding the origin of valence delocalization in  $\text{Cu}_A$  and **1**: The delocalization observed in **1** indicates that the value of  $2H_{\text{AB}} = 5600 \text{ cm}^{-1}$  is large relative to the vibronic trapping energetics of this dimer. Comparing the delocalization pathway of **1**, which contains significant S covalency but little or no direct Cu–Cu interaction, to that in the structurally-similar valence-trapped  $\text{S} = 1/2 [\text{Fe}_2(\mu\text{-S})_2]^+$  ferredoxins ( $2H_{\text{AB}} \approx 2000 \text{ cm}^{-1}$ ), which involves predominantly a direct Fe–Fe interaction and little or no Fe–S covalency,<sup>9,16</sup> shows that electronic coupling in **1** is indeed large and emphasizes that bridging superexchange contribution can be an efficient mediator of valence delocalization. Direct  $2.5 \text{ \AA}$  Cu–Cu bonding interactions in  $\text{Cu}_A$  more than double the magnitude of  $2H_{\text{AB}}$  relative to the already large value found in **1**, thus stabilizing the delocalization of  $\text{Cu}_A$  despite its lower-symmetry protein environment.

While no specific pathway for Cyt *c*  $\rightarrow \text{Cu}_A$  ET has been identified,  $\text{Cu}_A$  to heme *a* ET has been proposed to involve Cu–N(His) ligation<sup>1b,4c</sup> since this accesses the shortest pathway. Previous studies have shown that the rate of ET,  $k_{\text{ET}}$ , between a donor and an acceptor is proportional to  $(\alpha^2)^2$ .<sup>13b,c,17</sup> From this study,  $\alpha^2(\text{Cys}) \gg \alpha^2(\text{His})$  (13%/S(Cys) (Figure 1) vs  $\sim 1$ –3%/N(His) from ENDOR<sup>18</sup>), from which  $k_{\text{ET}}(\text{S(Cys)})/k_{\text{ET}}(\text{N(His)}) \approx 19$ –169. From this ratio and estimation of an ET decay parameter of  $\sim 0.6$  per covalent bond,<sup>19</sup> a S(Cys) ET pathway could contain  $\sim 5$ – $10$  covalent bonds more than a competing N(His) pathway and still achieve a comparable  $k_{\text{ET}}$ . Thus, the relatively high S(Cys) covalency in the  $\text{Cu}_A$  HOMO could contribute significantly to both Cyt *c*  $\rightarrow \text{Cu}_A$  and  $\text{Cu}_A \rightarrow$  heme *a* ET processes in CcO, analogous to the effects of anisotropic covalency observed in Pc ET kinetics.<sup>17</sup> It is interesting to note that  $\text{Cu}_A$  ET is faster than that of the blue copper center in the multicopper oxidases<sup>20</sup> despite  $\text{Cu}_A$  having reduced superexchange ligand covalencies and less efficient donor-to-acceptor ET pathways; this observation supports the possibility that the delocalized mixed-valence binuclear structure of  $\text{Cu}_A$  contributes significantly to its ET function.

**Acknowledgment.** This research has been supported by the NSF [CHE-9217628 (E.I.S.), CHE-9423181 (K.O.H.), and NYI award (W.B.T.)] and the NIH [RR-01209 (K.O.H.) and GM47365 (W.B.T.)]. SSRL operations are funded by the DOE, Office of Basic Energy Sciences. The Biotechnology Program is supported by the NIH, Biomedical Research Technology Program, National Center for Research Resources. Further support is provided by the DOE, Office of Health and Environmental Research.

JA963225B

(15) When compared to other first-row transition-metal dimers having unsupported M–M bonds, for which  $\sigma$ – $\sigma^*$  transition energies are typically  $> 25\,000 \text{ cm}^{-1}$ , the  $\sim 7400 \text{ cm}^{-1}$  Cu–Cu  $\sigma$ – $\sigma^*$  bonding interaction in  $\text{Cu}_A$  is seen to be relatively weak. See, for example: Abrahamson, H. B.; Frazier, C. C.; Ginley, D. S.; Gray, H. B.; Lilienthal, J.; Tyler, D. R.; Wrighton, M. S. *Inorg. Chem.* **1977**, *16*, 1554–1556.

(16) Noodleman, L.; Baerends, E. J. *J. Am. Chem. Soc.* **1984**, *106*, 2316–2327.

(17) Lowery, M. D.; Guckert, J. A.; Gebhard, M. S.; Solomon, E. I. *J. Am. Chem. Soc.* **1993**, *115*, 3012–3013.

(18) Gurbriel, R. J.; Fann, Y.-C.; Surerus, K. K.; West, M. M.; Musser, S. M.; Doan, P. E.; Chan, S. I.; Fee, J. A.; Hoffman, B. M. *J. Am. Chem. Soc.* **1993**, *115*, 10888–10894.

(19) (a) Beratan, D. N.; Onuchic, J. N.; Betts, J. N.; Bowler, B. E.; Gray, H. B. *J. Am. Chem. Soc.* **1990**, *112*, 7915–7921. (b) Beratan, D. N.; Betts, J. N.; Onuchic, J. N. *Science* **1991**, *252*, 1285–1288.

(20) Solomon, E. I.; Sundaram, U. M.; Machonkin, T. E. *Chem Rev.* **1996**, *96*, 2563–2605.

(21) The  $[\text{Cu}_2(\mu\text{-SR})_2]^+$  cores are depicted in the  $D_{2h}$  high-symmetry limit for clarity, although X $\alpha$ -SW calculations indicate a significant dependence of the MO description on the S–C orientation.<sup>14</sup> Reduction from  $D_{2h}$  symmetry relaxes the rigorous  $\sigma^b$ – $\sigma^*$  and  $\pi^b$ – $\pi^*$  MO descriptions depicted and, in particular, allows for mixing of Cu–S  $\sigma$ , pseudo  $\sigma$ , and  $\pi$  bonding interactions.

(14) Gamelin, D. R.; LaCroix, L. B.; Houser, R. P.; Tolman, W. B.; Mulder, T. C.; deVries, S.; Solomon, E. I. To be published.